Estimates of confinement time and energy gain for plasma liner driven magnetoinertial fusion using an analytic self-similar converging shock model

J. T. Cassibry,[1] R. J. Cortez,[1] S. C. Hsu,[2] and F. D. Witherspoon[3]

[1]*Propulsion Research Center, Technology Hall S-226, The University of Alabama in Huntsville, Huntsville, Alabama 35899, USA*
[2]*Physics Division, Los Alamos National Laboratory, Los Alamos, New Mexico 87545, USA*
[3]*HyperV Technologies Corp., Chantilly, Virginia 20151, USA*

Plasma liner driven magnetoinertial fusion (PLMIF) is a fusion energy concept that utilizes an imploding plasma liner to shock heat and compress a magnetized target plasma to fusion conditions. The fusion burn fraction is linearly proportional to the confinement (or "dwell") time of the liner-target system at peak compression, and therefore it is important to estimate the dwell time accurately in order to assess the fusion energy yield and gain. In this work, the dwell time has been estimated using the exact solution to a self-similar converging shock model. The dwell time was found to be determined by the sum of the outgoing shock and rarefaction times through the plasma liner at peak compression, and for chosen PLMIF conditions the dwell time was on the order of 1 μs. In addition, we show that the engineering gain, i.e., the total energy extracted as electricity (from fusion plus expanded liner energy) divided by the electrical energy required to implode the liner, exceeds unity for a wide range of liner thicknesses and specific heat ratios. © 2009 American Institute of Physics. [doi:10.1063/1.3257920]

I. INTRODUCTION

Magnetoinertial fusion (MIF) uses a magnetic field in an inertially confined fusing plasma to reduce thermal losses and to enhance alpha particle self-heating of the fuel. This reduces the areal density (ρr) threshold for ignition[1] allowing lower implosion velocities, or alternatively it allows higher gain for a given implosion velocity. The magnetized target fusion (MTF) approach[2–5] to MIF takes advantage of the former, while magnetized inertial confinement fusion takes advantage of the latter.[6] In the MTF approach, batch-burn fusion is sought at $\rho r \leq 0.01$ g/cm^2 by using a radially imploding material liner (typically driven by pulsed power) to compress and heat a magnetized target plasma.

Of paramount importance to the success of the MTF approach is the liner. Solid liner implosion technology for MTF is a fairly mature research effort.[7] Experiments at AFRL-Kirtland routinely demonstrate magnetically driven implosions of solid metal liners with good symmetry to velocities of 10 km/s and a radial convergence factor of 10. Most recently, the first successful demonstration of an imploding solid liner with geometric scale lengths and compression ratios suitable for compressing a field reversed configuration target was achieved.[2] Radiographs indicated a 13 times radial compression ratio with no observable instability growth. But solid liners may suffer from potential engineering difficulties in the context of a reactor concept due to reasons such as nonreusability, manufacturing costs, and debris deposits along the interior of the wall.[8]

Plasma liner driven magnetoinertial fusion (PLMIF)[8,9] aims to overcome these problems at the expense of requiring a higher implosion velocity (on the order of 100 km/s compared with solid liners (requiring ≤ 10 km/s) and lower hydrodynamic efficiency due to increased liner thickness. PLMIF has the primary benefit of potentially allowing all the driver hardware to be situated far enough away so that they are not destroyed during each shot, i.e., imploding plasma liners are a potential solution to the "stand-off" problem. The drivers could be, for example, pulsed plasma accelerators,[10] and other drivers such as plasma streams used as disposable electrodes[11] have been considered. Since the liner can be created by the formation and merging of plasma jets, the system is highly repeatable, eliminating the need to manufacture a liner for each shot.

A. Plasma liner driven magnetoinertial fusion

In PLMIF a cylindrical or spherical plasma shell implodes onto and compresses a magnetized plasma. Once the liner has been formed and has reached the outer boundary of the target, the evolution of the target and shock boundaries can be described in five stages (1–5), as illustrated in Fig. 1. One can also identify four distinct regions (A–D) which can be defined by either the target/liner interface or a shock. It should also be noted that this is an idealized representation, and an actual system may be complicated by, among other things, gradients in the flow field, asymmetries, and the possibility of a greater number of internal shocks. We are also assuming that this is a collision dominated hydrodynamic process, since electron-ion collision times are ~1 ns while the implosion/expansion time scale is ~1 μs. Setting the complications aside, the five stages are the following:

(1) The plasma liner (region D) implodes from the radius at which it is formed to the target radius. Both the target (region A) and the liner are otherwise undisturbed. The
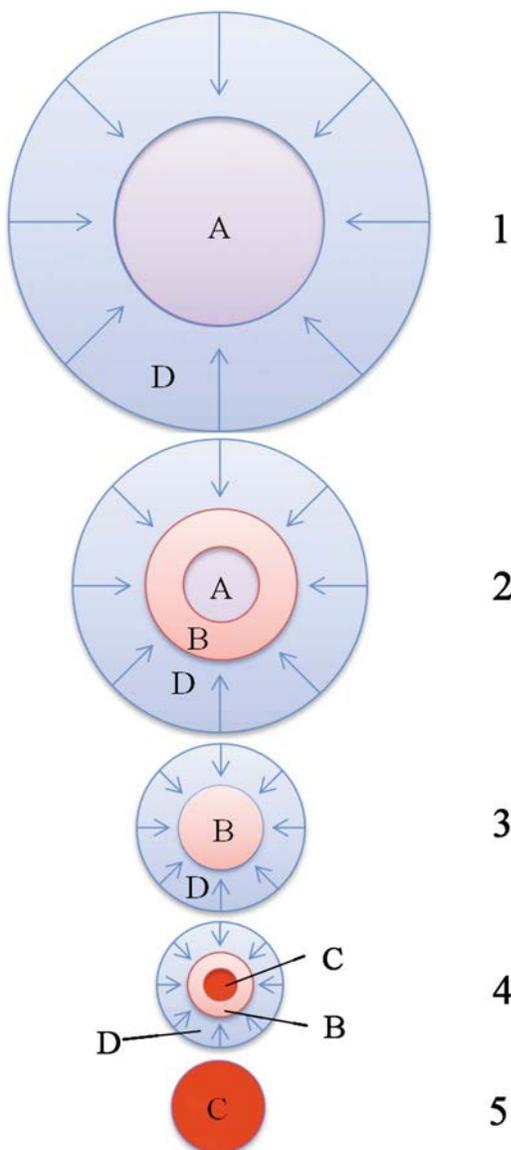
FIG. 1. (Color online) Stages (1–5) of target and liner compression in PLMIF.

C) will reach the highest temperatures and pressures during the process. Once the reflected shock reaches the target/liner boundary, it will either reflect inward or continue outward. The inward/outward reflected shocks become progressively weaker[8] until the rising inner target pressure matches the incoming dynamic pressure of the liner, at which time a stagnation shock will propagate radially outward through the liner. The number, if any, of the secondary converging/reflected shocks will depend on the strength of the mismatch between the high dynamic pressure of the liner and the relatively low static pressure of the target.

(5) The liner has completely stagnated, and the entire system behind the final outgoing shock is denoted as region C, Fig. 1.

Beyond stage 5, a rarefaction wave will travel radially inward, disassembling the stagnated liner/target system. Once the wave has reached the origin, the target will no longer be confined. The dwell time, as a function of liner thickness, is therefore approximated as the duration of the outgoing shock through the target and liner (beginning at stage 3, i.e., point of peak compression) plus the time of the rarefaction wave (after stage 5). Even though the fusion burn may actually start a few tens of nanosecond before peak compression, we choose this point out of convenience and to remain conservative in the dwell time calculation.

The physics basis for PLMIF has been explored by Thio *et al.*[11] and Knapp,[12] and the formation of imploding plasma liners using merging high Mach number plasma jets was proposed by Thio *et al.*[9] Los Alamos National Laboratory's SPHINX code was used for the modeling effort.[12] The modeling results indicate that the jets can form a stable, imploding liner both in a cylindrical and spherical distribution and compress a target to thermonuclear conditions.[13]

Chen *et al.*[14] explored the stability of spherically imploding shocks using an unsteady self-similar solution. Growth rates of the amplitudes of the perturbations exhibited a power law rather than more deleterious exponential behavior during convergence, and the amplitudes decrease to zero as the shock waves reach the origin. The main conclusion reached was that imploding shock waves are stable near shock collapse. The spherical pinch experiment[15] was an outgrowth of earlier cylindrical experiments, which built upon the observation that cylindrically imploding shock waves were stable. Confinement of the central plasma hot spot exceeded 5 μs in some cases.

Zero-dimensional (0D) and one-dimensional (1D) models have been developed by Thio.[8,16] In the 0D code,[8] the implosion dynamics has been studied in three phases: the preliminary shock heating and compression, the acoustic compression, and the confinement of the burning target and liner. Results show that plasma jet driven MIF has a potential for wall-plug gain of greater than 50, with pulsed power drivers available at existing state-of-the-art facilities. The 1D Lagrangian model[16] showed that the target ignition and burn can be achieved in a target of a 1 mg plasma, 10 cm initial diameter imploded by a plasma liner with about 1 g of material, target magnetic field of 10 T, and implosion velocity

arrows indicate the radially inward motion of the liner. In Fig. 1, stage 1 depicts the moment at which the liner impacts the target.

(2) A radially inward shock is launched at the target/liner interface, provided the liner velocity (v_l) exceeds the local target sound speed. For a 50/50 Deuterium/Tritium (DT) mixture, this criterion is $v_l > 254 T_{keV}^{1/2}$ [km/s], requiring $v_l > 80$ km/s for a 0.1 keV target. A shocked layer of target material (region B) forms behind the shock and travels inward. Liner compression (region D) continues throughout stages 1–4 and is primarily isentropic.

(3) The shock reaches the origin, and the target has now been entirely shock heated. Region A has been entirely replaced with region B via the converging shock.

(4) Immediately after shock collapse at stage 3, a reflected shock in the radially outward direction is launched. The inner target material behind the reflected shock (region

of about 250 km/s. Without the magnetic field, the target temperature was limited to about 1 keV. The latest thinking points to using a high Z liner with afterburner, in which case the target magnetic field should be lowered to allow some alpha particles to escape and heat the afterburner.[17]

More recently, Parks[18] developed a new theoretical model to estimate liner criteria for plasma jet driven magnetoinertial fusion. The peak pressure was shown to be strongly dependent on the incoming ram pressure, as $\sim C^2$, where C is the convergence ratio defined as the merging radius divided by the stagnation radius. Furthermore, the dwell time was shown to be $R/2u_j$, where R is the target radius and u_j is the liner velocity. This result significantly limited the fusion gain since the dwell time was estimated to be on the order of 100 ns. A key result of the present paper is to show that the dwell time estimated using a converging shock model is closer to 1 μs.

B. Outline

In this paper, we use the exact solution to the self-similar converging shock model to estimate the dwell time. We choose the converging shock model because it is an exact solution to a subset of cases in the rich PLMIF parameter space. The self-similar model and its relevance to PLMIF are described in Sec. II. Numerical results of the model are presented in Sec. III, and these are used to estimate the dwell time based on the duration from peak compression to expansion of twice the compressed radius in Sec. IV. In Sec. V, we argue that the engineering gain, the total energy extracted as electricity (from fusion plus expanded liner energy) divided by the electrical energy required to implode the liner, is a more relevant figure of merit for reactors than fusion gain, which ignores the expanding plasma liner as a source of energy. We will show that even without including the fusion power output, engineering gain is a significant fraction of unity. A summary is given in Sec. VI.

II. SELF-SIMILAR MODEL

For a uniform gas at rest obeying the adiabatic (constant gamma) ideal gas law, there is a similarity solution for an infinite Mach number shock converging on the origin in cylindrical and spherical symmetry.[19–21] Below we discuss the relevance of this solution to PLMIF, and we summarize the self-similar solution to the converging shock problem for completeness (as presented by Lazarus and Richtmeyer[20] in a technical report and later formalized by Lazarus[22]). Finally, we discuss the application of the solution to our problem and the scope of its applicability.

A. Relevance of converging shock model to PLMIF

The physics of the converging shock problem is very similar to that of a liner imploding on an adiabatic target, which is why it was chosen to give insights into PLMIF confinement. The solution can be described referencing a plot of the incoming and reflected shock trajectory, Fig. 2. Region A is an undisturbed region of uniform gas located about $r=0$, into which a radially imploding shock is propa-
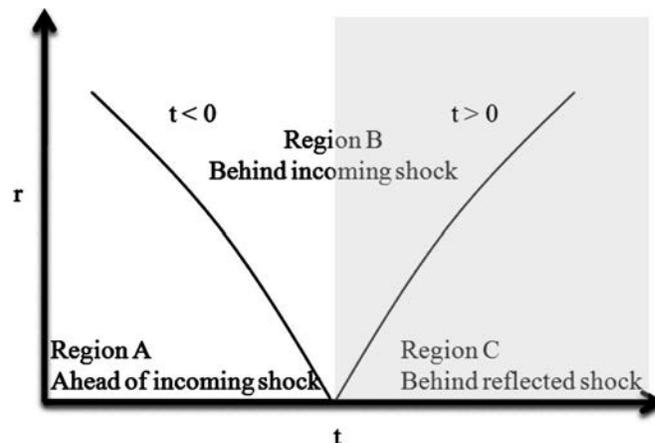

FIG. 2. *r-t* trajectories of incoming and reflected shocks.

gating. For all $t<0$, behind the incoming shock, the solution to region B describes the radially imploding gas which has been shock heated, compressed, and accelerated by the shock. At $t=0$, the incoming shock collapses on the origin. An outgoing shock is produced by the reflection at the origin, and for $t>0$, there exists a region C for which the solution describes the flow behind the outgoing reflected shock. These regions (A–C) in Fig. 2 are identified in the same manner as those in Fig. 1 to show that the convergence of a shock onto an undisturbed cylindrical column or sphere of gas followed by the reflection of the shock at the origin is common to both the converging shock solution and PLMIF.

There are some differences between the converging shock and PLMIF problems. The converging shock problem has only three distinct stages, and they are illustrated in Fig. 3 and described as follows:

(1) A converging shock implodes toward the center and shock heats an undisturbed region of gas (region A). The shocked gas extends to infinity and is denoted as region B. This is similar to stage 2 of Fig. 1, without a finite, imploding liner (region D) driving the shock. The model assumes that the liner Mach number (with respect to the target sound speed) is infinite, and therefore the temperature in region A is assumed to be negligible. Consequently, the density jump across the shockwave into region B is $\sim(\gamma+1)/(\gamma-1)$ in accordance with the hypersonic limit, and the shocked pressure is $\mathcal{O}(\rho v_l^2)$, where v_l is the liner velocity. The pressure and density will be somewhat lower in region B in a PLMIF target with finite temperature, depending on the local sound speed and liner velocity.

(2) The shock reaches the origin, and the target has now been entirely shock heated. Region A has been entirely replaced with region B via the converging shock.

(3) Immediately after shock collapse at stage 2, a radially outward shock is launched. The inner target material behind the reflected shock (region C) will reach the highest temperatures and pressures during the process. Since there is no outer boundary, the outgoing shock propagates into the incoming gas toward infinity for all $t>0$. It is important to note that the density and pressure are
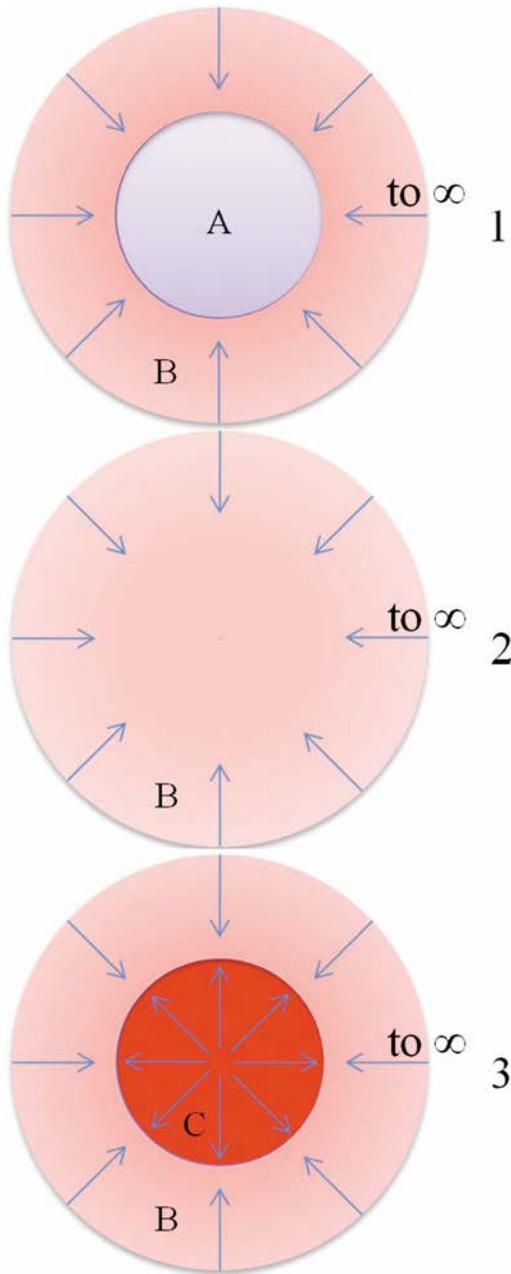
FIG. 3. (Color online) Stages (1–3) of solution to the self-similar converging shock problem.

greatly amplified in region C behind the second shock.

Thus, the main qualitative differences between PLMIF and the converging shock solution are that the PLMIF system has finite boundaries and a separate liner (region D) which drives the imploding shock, and the initial "target" in the converging shock solution has negligible temperature. Additionally, the converging shock solution neglects the effect of an adiabatic target on the liner kinematics following the radial shock implosion at the origin. It has been shown elsewhere[18] that the hydrodynamic efficiency of liner energy coupled to the target is only ~1%–5% for PLMIF. Thus, the target introduces only a small perturbation to the liner kinematics and may be neglected in the present study where high precision is not sought. Nevertheless, the physics of shock

heating the undisturbed region A is identical in both cases, presuming that the liner velocity exceeds the target sound speed in the PLMIF case. We use the solution to the converging shock model to gain insights into the expansion velocity of the target behind the outgoing shock (region C), the rarefaction time of the shocked target, relative shock and liner velocities, and dwell time based on the liner shock time plus the rarefaction time.

B. Solution of the converging shock model

The governing partial differential equations (PDEs) for 1D cylindrical or spherical problems are

$$\frac{\partial \rho}{\partial t} + \frac{\partial(\rho u)}{\partial r} + \frac{\nu \rho u}{r} = 0, \tag{1}$$

$$\frac{\partial u}{\partial t} + u\frac{\partial u}{\partial r} + \frac{1}{\gamma \rho}\frac{\partial}{\partial r}(\rho c^2) = 0, \tag{2}$$

$$\frac{\partial c}{\partial t} + u\frac{\partial c}{\partial r} + (\gamma - 1)c\left(\frac{\partial u}{\partial r} + \frac{\nu u}{r}\right) = 0, \tag{3}$$

where $\nu = 1, 2$ for cylindrical, spherical symmetry, r is the spatial (radial) coordinate, ρ is the mass density, u is the velocity, γ is the specific heat ratio, and c is the sound speed. Equations (1)–(3) represent conservation of mass, momentum, and energy, respectively. Using the free parameters α and κ and trying the similarity variable

$$y = C + \ln r = \alpha \ln t \tag{4}$$

and the substitutions

$$u(r,t) = -\frac{\alpha r}{t}V(y), \tag{5}$$

$$c(r,t) = -\frac{\alpha r}{t}C(y), \tag{6}$$

and

$$\rho(r,t) = \rho_0 r^\kappa R(y), \tag{7}$$

the following three equations can be derived:

$$R' + (\kappa + \nu + 1)RV + (RV)', \tag{8}$$

$$V(\lambda + V) + V'(1 + V) + \frac{C}{\gamma}\left[(\kappa + 2)C + C' + \frac{C'}{R}\right], \tag{9}$$

$$2C(\lambda + V) + 2C'(1 + V) + (\gamma - 1)C[(\nu + 1)V + V']. \tag{10}$$

Equations (8)–(10) are coupled ordinary differential equations (ODEs) which describe the self-similar behavior for continuous flow. Since this problem involves two discontinuities, it has to be divided into three distinct regions (as shown in Fig. 2). Out of convenience, since the ODEs of the model are independent of y, Lazarus and Richtmeyer

changed to the similarity variable $x = -e^{y/\alpha}$. For a converging shock, a similarity solution requires that a shock be at a constant value of the similarity variable x, so that the physical boundary condition along the shock trajectory $r_{shock} = r(t)$ can be a boundary condition at some initial value of the similarity coordinate x for the ODEs. Accordingly, the shock trajectory must be described by

$$r_{shock} = A(-t)^{\alpha}, \tag{11}$$

so that the shock path is $x = -1$. In terms of the similarity variables V, C, and R, the jump conditions across the shock are

$$1 + V_1 = \frac{\gamma - 1}{\gamma + 1}(1 + V_0) + \frac{2C_0^2}{(\gamma + 1)(1 + V_0)}, \tag{12}$$

$$C_1^2 = C_0^2 + \frac{\gamma - 1}{2}[(1 + V_0)^2 - (1 + V_1)^2], \tag{13}$$

$$R_1(1 + V_1) = R_0(1 + V_0). \tag{14}$$

There are several challenges involved in obtaining a proper solution. First, Eqs. (8)–(10) need to be decoupled and put into a form which guarantees physical behavior. Specifically, the solution must extend through $x = 0$, and V and C must be zero at $x = 0$. Second, the equations have to be integrated separately in the reflected shock zone, and the two solutions must satisfy the jump conditions at the shock boundary according to Eqs. (12)–(14). Finally, both regions 2 and 3 have singularities that can occur during the integration, so the free parameters need to be chosen judiciously to avoid numerical difficulties. To accomplish this, Lazarus and Richtmyer used different but equivalent forms of the decoupled ODEs in each of the regions, which could be reduced to two functions of C and V only. Each set was designed to give good behavior required in regions 2 and 3. Once a solution is obtained for V and C, the physical variables v and c can be calculated with Eqs. (5) and (6). The density in region 2 was shown to be[20]

$$\rho_2(r,t) = \rho_2(x) = \frac{\gamma + 1}{\gamma - 1}\left[\frac{x_0}{x}\frac{C_2(x)}{C_2(x_0)}\left(\frac{1 + V_2(x)}{1 + V_2(x_0)}\right)^a\right]^b, \tag{15}$$

where $x_0 = -1$,

$$a = \frac{1 - \alpha}{\alpha(\nu + 1)}, \tag{16}$$

and

$$b = \frac{2\alpha(\nu + 1)}{[\gamma(\nu + 1) - (\nu - 1)]\alpha - 2}. \tag{17}$$

Behind the reflected shock in region 3, the density is[20]

$$\rho_3(r,t) = \rho_3(x) = \rho_3(\beta)\left[\frac{\beta}{x}\frac{C_3(x)}{C_3(\beta)}\left(\frac{1 + V_3(x)}{1 + V_3(\beta)}\right)^a\right]^b. \tag{18}$$

For the numerical integration of the converging shock model it was necessary to use the boundary conditions in Eqs. (12)–(14) in order to create continuity across the shock at $t = 0$. For the region behind the incoming shock, the indepen-

dent variable used was $x = t(A/r)^{\lambda}$, and the dependent variables were $v(x) = -V(x)/x$ and $c(x) = C(x)/x$. The division by x gives nice behavior at the singularity $V = C = 0$. Using $x = -1$ as the initial value, the integration must proceed past $x = \beta$, where β is unknown. As an effective way of handling the unknown value of β, the equations were used in the form $dv/dx = N_1(V,C)/D(V,C)$ and $dc/dx = N_2(V,C)/D(V,C)$, where

$$D(V,C) = (1 - vx)^2 - (cx)^2, \tag{19}$$

$$N_1(V,C) = p_1[v^2(1 - vx) + p_2c^2] - p_3vc^2x, \tag{20}$$

$$N_2(V,C) = c\left[v(p_5 - p_{20}vx) + p_1c^2x\left(1 - \frac{p_2}{2(1 - vx)}\right)\right],$$

and the constants were

$$p_1 = 1 - \alpha,$$

$$p_2 = \frac{2}{\gamma},$$

$$p_3 = (\nu + 1)\alpha - 1, \tag{21}$$

$$p_5 = \tfrac{1}{2}[(\gamma + 1)(1 - \alpha) - \alpha\nu(\gamma - 1)],$$

$$p_{20} = 1 - \alpha - \frac{\alpha\nu}{2}(\gamma - 1).$$

For the region behind the reflected shock, the independent variable used was $t = kx^{-\sigma}$, where k is a free parameter that cancels out of the differential equations and σ is defined by

$$\lambda\sigma = 1 + \frac{(\nu + 1)(\lambda - 1)}{(\nu + 1)\gamma - 2(\lambda - 1)}. \tag{22}$$

The dependent variables were $v(t) = -V(x)$ and $c(t) = C(x) + 1/t$, and the differential equations were used in the form $dv/dt = M_1/\sigma tE$ and $dc/dt = 1/t^2[-1 + (1 - ct)M_2/\sigma E]$, where

$$E = (1 - ct)^2 - (1 - v)^2t^2,$$

$$M_1 = v(1 - v)(1 - \alpha v)t^2 - p_4(1 - ct)^2(v - p_6), \tag{23}$$

$$M_2 = (1 - ct)^2\left(\alpha + \frac{p_{21}}{1 - v}\right) - t^2[(1 - v)(1 - p_{22}v) + p_{23}v],$$

and the corresponding constants are

TABLE I. Specific heat ratios (γ) and corresponding self-similar coefficients for cylindrical ($\nu=1$) and spherical ($\nu=2$) implosions.

$\nu=1$		
γ	α	β
1.1	0.885 248 06	13.5364
1.4	0.835 323 20	2.815 61
1.67	0.815 624 90	1.694 79
$\nu=2$		
γ	α	β
1.1	0.795 969 80	16.1541
1.4	0.717 174 50	2.688 49
1.67	0.688 376 82	1.547 90

$$p_4 = \alpha(\nu + 1),$$

$$p_6 = 2\frac{1-\alpha}{\alpha\gamma(\nu+1)},$$

$$p_{21} = \frac{(1-\alpha)}{\gamma}, \quad (24)$$

$$p_{22} = \alpha\left(1 + \tfrac{1}{2}\nu(\gamma-1)\right),$$

$$p_{23} = \tfrac{1}{2}(\gamma-1)(1-\alpha).$$

The integration is carried out until $V=-\nu$ and $C=c-1/t$ match the target functions. The interpolated value of x at which the match occurs is then β.

C. Scope of study

The values of α and β used were calculated by Lazarus and Richtmeyer according to the values of $\gamma=1.1$, 1.4, 5/3, for both cylindrical and spherical symmetries ($\nu=1,2$), giving six permutations to study. Each solution represents a family of solutions for which the undisturbed material density ahead of the incoming shock was varied as $\rho_1=4.15 \times 10^{-6}$ to $\rho_1=4.15$ kg/m^3 (10^{21} to 10^{27} ions/m^3 in increments of 1 in $\log_{10}$ space). Table I summarizes the specific heat ratios and corresponding self-similar coefficients (taken from Ref. 22) for both cylindrical ($\nu=1$) and spherical ($\nu=2$) symmetries. For each of the cases, the implosion velocity was varied as 50, 100, 200, and 400 km/s. Since the incoming velocity is not constant with radius, we set A in Eq. (11) to give the specified velocity at the leading edge behind the incoming shock on the time scale $0.01/v_l$ [s]. All cases were set up as iterations of every permutation of the chosen parameters.

III. NUMERICAL RESULTS

For illustrative purposes, we plot velocity, temperature, density, and pressure vs. radius at fixed time. The temporal and spatial evolution of the flow field is qualitatively the same in all cases, so we restrict the discussion to one case,

$\nu=2$ (spherical symmetry), $\gamma=1.67$, $v_l=200$ km/s, and target density of 10^{23} m^{-3}. A 50/50 mixture of deuterium/tritium is assumed, so the molecular weight is 2.5 kg/kmol. For negative/positive time, the shock is propagating inward/outward, respectively. The results are shown in Fig. 4 for -50, -25, 25, and 50 ns.

At -50 ns, the leading edge of the incoming shock is moving at ~ 200 km/s and is physically located at ~ 2 cm, Fig. 4(a). In 25 ns at constant speed, the liner would have moved 5 mm, however, the liner *accelerates* into the origin and has instead moved 8 mm. The acceleration is caused by a pressure gradient across the incoming shock which increases with $1/r^\nu$. To a good approximation, the kinetic energy of the liner is converted entirely into thermal energy across the shock, giving a leading edge temperature of $v_l^2/(3R)$, Fig. 4(b). The density jump is $\sim (\gamma+1)/(\gamma-1)$ in accordance with the jump conditions in the hypersonic limit. The static pressure behind the shock is roughly equal to the dynamic pressure, and is not independent of T and ρ.

For $t>0$, the shock propagates radially outward. The velocity varies from 0 at the origin to a maximum (about 20% of the incoming liner velocity) and then drops sharply negative across the outgoing shock, Fig. 4(a). A singularity exists at the origin, and the solution gives $T\to\infty$ as $r\to 0$. T decreases monotonically with r, dropping sharply across the shock, Fig. 4(b). While empirical, we have found that the peak density is approximately $\rho_0[(\gamma+1)/(\gamma-1)]^{-0.7602\gamma^2+1.334\gamma+2.393}$, where ρ_0 is the undisturbed target density. The density tends toward 0 as $r\to 0$. The pressure is fairly constant behind the shock, Fig. 4(d), but displays a mild pressure gradient toward the origin which causes deceleration of the flow behind the outgoing shock, Fig. 4(a).

IV. ESTIMATION OF DWELL TIME USING THE SELF-SIMILAR SOLUTION

There are four characteristic velocities of interest during confinement, the expansion speed of the target (v_e), the rate of propagation of the outgoing shock wave through the liner (v_s), the incoming liner velocity (v_l), and the rarefaction velocity (v_r). While the shock wave propagates to the edge of the liner, the target expands at velocity v_e from the compressed target radius r_t to an expanded radius of r_e. The exact solution of the self similar model shows the relative expansion velocity, v_e/v_l is only ~ 1 to 2%, Fig. 5.

Since v_e is relatively small, the compressed target does not expand significantly until after the rarefaction wave reaches the target. Thus, we approximate the dwell time (τ) in PLMIF as the duration *from* peak compression *to* the outgoing shock reaching the outer liner boundary (liner compression time) *plus* the rarefaction time,

$$\tau \approx \frac{\ell}{v_s - v_l} + \frac{\ell_c + r_e}{v_r}, \quad (25)$$

where v_l is negative, ℓ is the uncompressed liner thickness, and ℓ_c is the compressed liner thickness. To be conservative, we can neglect the rarefaction time. Further, since the self-similar model gives $v_s \sim -v_l$, we can simplify Eq. (25) to
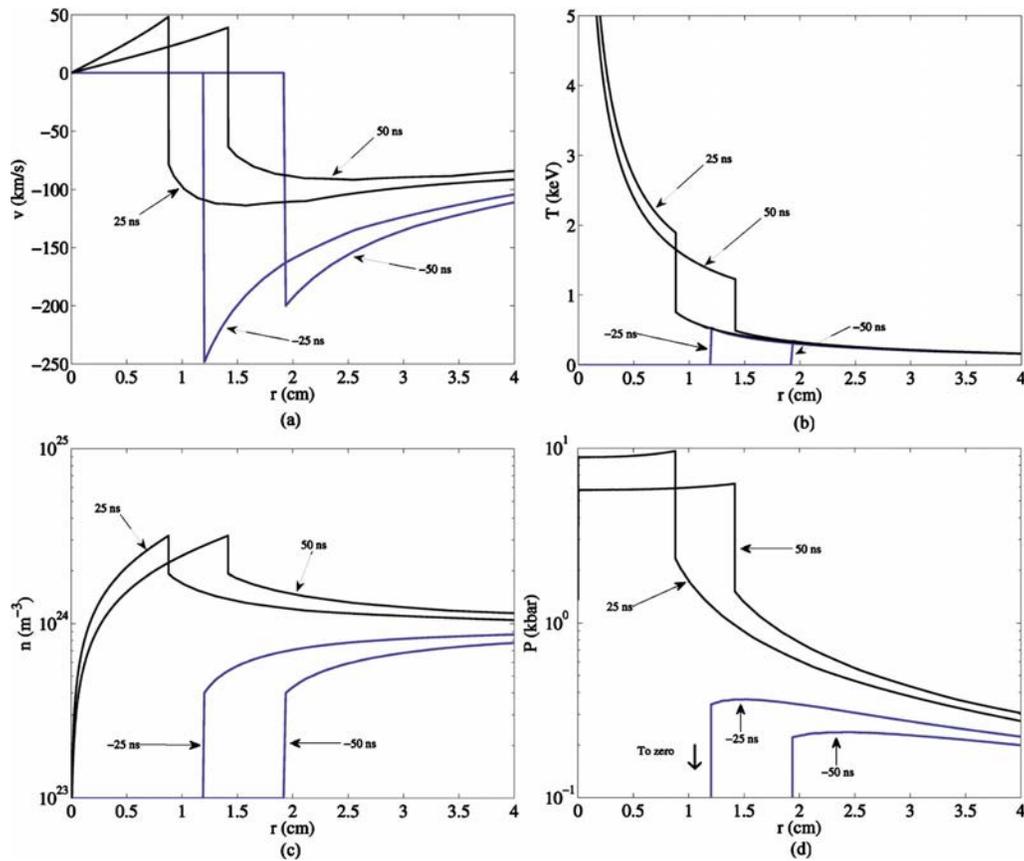
FIG. 4. (Color online) (a) Velocity, (b) temperature, (c) density, and (d) pressure vs radius at fixed times before (negative time) and after (positive time) shock collapse.

$$\tau \approx \frac{\ell}{2|v_l|} \qquad (26)$$

For a liner thickness of 0.15 m and v_l of 100 km/s, this gives a dwell time of 750 ns.

To strengthen our argument that Eq. (26) is a conservative estimate for the dwell time, we can calculate the dwell time using Eq. (25) and the time dependent solution to the
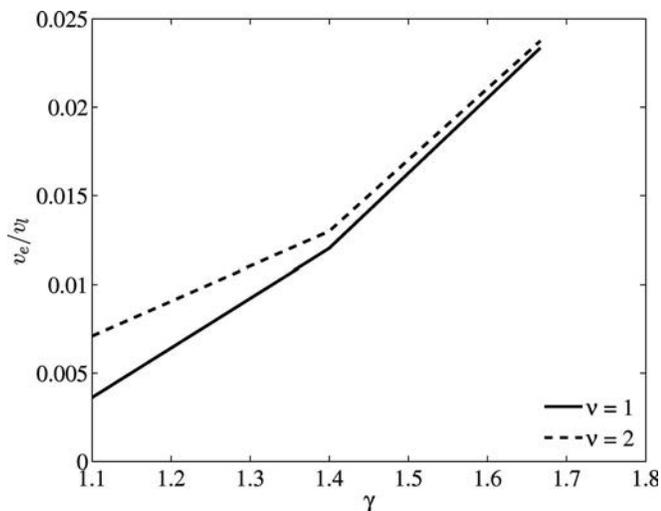

FIG. 5. Relative expansion velocity normalized against incoming liner velocity.

converging shock solution. To make this calculation, one has to assume an initial target radius and liner thickness. The target boundary describing the compressed radius is then tracked in the solution by assuming the target mass is constant. The start time t_s from which we compute the dwell time is found in the solution when the outgoing shock passes the compressed target radius. The dwell time is then calculated to be $t_l - t_s + dt_r$ where t_l is the time that the shock reaches the prescribed liner thickness and dt_r is the rarefaction time. dt_r is estimated using the local sound speed at the 'liner' edge just behind the outgoing shock at t_l and the outer radius of the compressed liner.

The results are shown below for an initially uncompressed target radius of 5 cm and a liner thickness of 15 cm, Fig. 6. The dwell time decreases monotonically with liner velocity as expected. As γ increases beyond 1.1, dwell time increases, but the results are nearly identical for 1.4 and 1.67. While not shown, we found the dwell time to be insensitive to the choice of target radius and to be linear with the prescribed liner thickness. For a liner velocity of 100 km/s, we calculated a dwell time of 4.7 μs with Eq. (25). This is considerably higher than the 750 ns result of Eq. (26). The primary reason for the longer dwell time is due to the slowing down of the incoming flow as both r and t increase in the solution. Real systems may actually behave as the solution. Liner expansion (in both directions) will be significant if the Mach number is of the order of 1, and the inner and outer liner edges will accelerate and decelerate, respectively in the
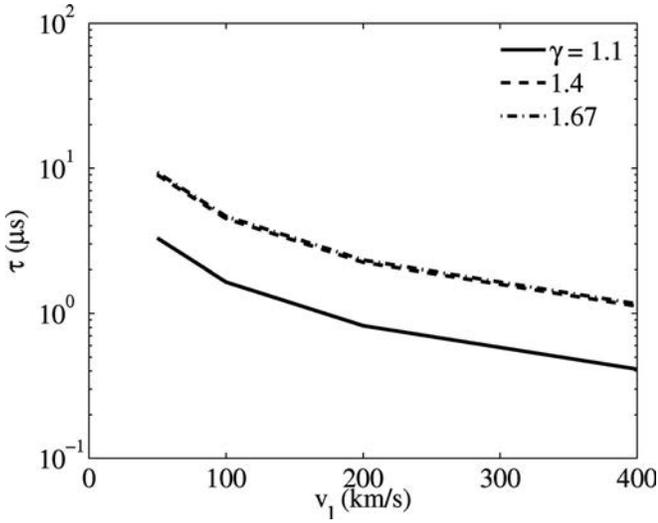
FIG. 6. Dwell time determined from the self-similar model and Eq. (25).

reference frame of the target boundary thereby increasing the dwell time in comparison with Eq. (26).

It is of interest to remark on the expansion ratio of the target during liner compression. This was determined numerically to be independent of the liner velocity and initial density and very insensitive to γ and ν. With better than 10% accuracy, the expansion ratio was 1.7 for all cases. Collectively, our results show dwell times may realistically approach 1 μs.

V. ENGINEERING GAIN VERSUS FUSION GAIN

Finally, we remark on the distinction between fusion and engineering gain. For complete fuel burn-up and 100% subsystem efficiencies, it has been shown that the gain G is 292.[18] In general, for a 50/50 mixture of deuterium/tritium fuel when one includes the neutron energy and accounts for the charged particle and thermal energy conversion efficiencies, the fusion gain is

$$G_{fusion} = \frac{(\eta_c 3.5 \times 10^3 + \eta_t 14.1 \times 10^3)}{3T_{keV}} f_b \eta_H \eta_{E_d}, \quad (27)$$

where η_c is the charged particle conversion efficiency, η_t is the thermal conversion efficiency, η_{E_d} is the electrical driver efficiency, η_H is the hydrodynamic efficiency, and the burn-up fraction, f_b, is given by

$$f_b(\tau) = \frac{1}{\left[1 + 1/\left(\frac{n\tau\langle\sigma v\rangle_{DT}}{2}\right)\right]}. \quad (28)$$

Note that f_b reduces to $f_b(\tau) \approx (n\tau\langle\sigma v\rangle_{DT}/2)$ when $(n\tau\langle\sigma v\rangle_{DT}/2) \ll 1$. The hydrodynamic efficiency, which is the efficiency in transferring liner to target energy, is given by (see Ref 18, Eq. 37)

$$\eta_H = \frac{R}{\ell}\left(\frac{\gamma-1}{\gamma+1}\right)^{1/2} \{1/\gamma + [1 + \gamma + \sqrt{17 + \gamma(2+\gamma)}]/4\}$$
$$\times \left[1 + \frac{2}{(\gamma-1)M^2}\right]^{1/2}, \quad (29)$$

where R is the target radius, ℓ is the liner thickness, M is the liner mach number, and γ is the specific heat ratio. This efficiency has been shown to be very low ($\sim$1%–5%) for PLMIF.[18] If the desired compressed target state is known, then this efficiency helps to establish liner criteria needed for ignition, and energy recovery from the expanded liner following the fusion burn becomes an important reactor consideration. In a fusion-based power plant, the liner energy would be converted to electricity by whatever means balances the additional infrastructure costs against the economical benefits of electrical power production. Thus, an overall engineering gain accounting for liner energy recovery must be devised in order to assess the feasibility of the concept.

While the archetype of the best configuration is yet to be envisaged, the choices of transduction include flux compression of the expanding plasma against an applied magnetic field and/or the thermal energy conversion using a Rankine cycle, Brayton cycle, or other thermal-to-electric conversion system. The charged particle conversion efficiency η_c can be estimated as $\sim$50%, which is limited by the resistive losses in the inductive recapture circuits and irreversibilities in the compression of the charged particles against the magnetic field. The thermal conversion efficiency is limited by the Carnot efficiency and the maximum effective heat transfer temperature at the system boundary, and will typically result in $\eta_t \sim$30%.

For the flux compression portion of energy recovery due to the expanding plasma liner, the target/liner system rarefaction speed can be approximated as the sound speed,

$$c_{system} \approx \sqrt{\gamma R_{gas} T_{system}}. \quad (30)$$

The actual velocity will exceed the sound speed by some factor up to $2/(\gamma-1)$.[23] Loosely defining the "temperature" of the system by

$$T_{system} = \frac{E_{system}}{m_{system} R_{gas}}(\gamma-1), \quad (31)$$

the kinetic energy of the expanding system is then

$$KE = 0.5 m_{system} c_{system}^2$$
$$= 0.5 m_{system} \gamma R_{gas} \frac{E_{system}(\gamma-1)}{m_{system} R_{gas}}$$
$$= 0.5\gamma(\gamma-1)E_{system}. \quad (32)$$

If we define the maximum liner recovery gain (G_{liner}) of the system as the kinetic energy divided by the system energy, it reduces to

$$G_{liner,max} = 0.5\gamma(\gamma-1), \quad (33)$$

which is a function only of the specific heat ratio. This function is plotted from γ=1.1 to 5/3, Fig. 7, which indicates that the liner energy does not have to be wasted; a significant
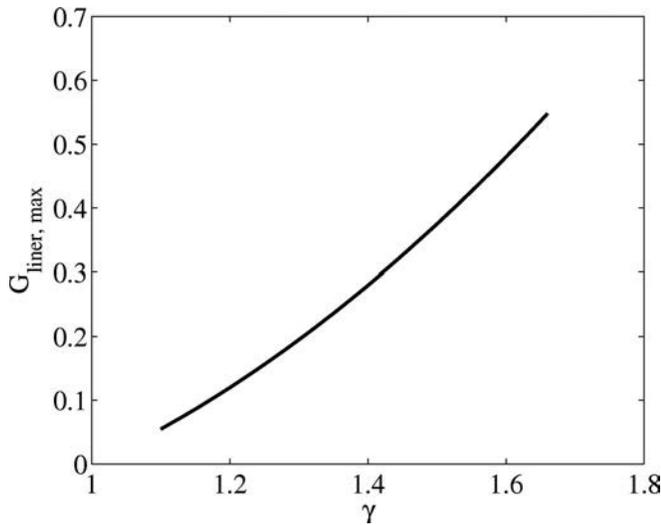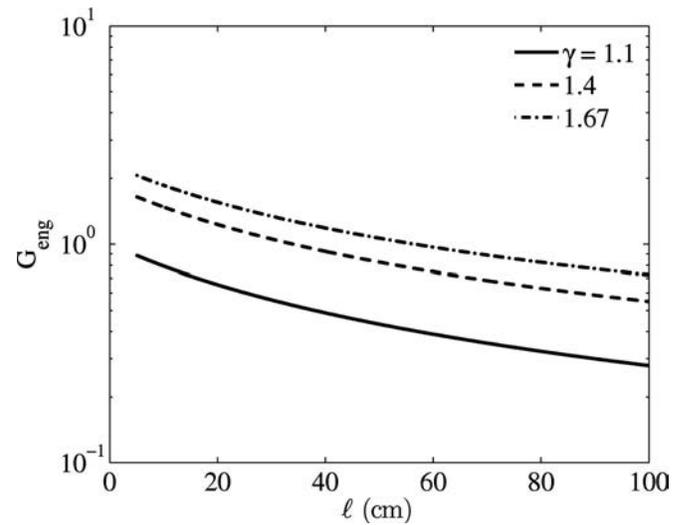
FIG. 7. Engineering gain vs specific heat ratio.

FIG. 8. System gain vs plasma jet length (ℓ) for a merging Mach number of 60.

fraction is available for producing work and monotonically increases with γ.

Neglecting the thermal and radiative energy recovery from the liner, the total engineering gain for the reactor would be the contributions from both fusion and liner energy recovery given by

$$
\begin{aligned}
G_{\text{eng}} &= G_{\text{fusion}} + G_{\text{liner,max}} \eta_{E_d} \eta_c \\
&= f_b(\tau) \eta_H \eta_{E_d} \left(\frac{\eta_c 3.5 \times 10^3 + \eta_t 14.1 \times 10^3}{3 T_{\text{target,keV}}} \right) \\
&\quad + 0.5 \gamma (\gamma - 1) \eta_{E_d} \eta_c.
\end{aligned} \tag{34}
$$

The electrical driver efficiency for a pulsed plasma accelerator with inductive recapture should be about 50% on a full scale reactor. To justify this assumption, other pulsed power plasma accelerators have demonstrated similar or higher efficiencies. For example, the pulsed inductive thruster (PIT) has reported 50% efficiency over a wide operating range.[24,25] Railguns with inductive recapture have reported even higher efficiencies.[26]

Using $\eta_t = 0.3$, $\eta_{E_d} = 0.5$, $\eta_c = 0.5$, $R = 0.5$ cm, $M = 60$, $n = 10^{28}$ m^{-3}, and $T_{\text{target,keV}} = 10$ keV, varying ℓ from 5 to 100 cm, and calculating τ with Eq. (26), $f_b(\tau)$ with Eq. (28), and η_H with Eq. (29), we can plot G_{eng} versus ℓ, Fig. 8. First we note that system gain decreases monotonically with liner thickness while increasing with γ. However, choosing $\ell = 15$ cm and $\gamma = 1.67$, the gain is 1.692. There are several reasons leading to an engineering gain that exceeds unity. First, we have shown that the dwell time is dominated by the outgoing shock propagation time through the liner, not the target, and therefore is not independent of jet length. This makes the engineering gain much less sensitive to jet length than the fusion gain. Second, we have included the thermal to electric conversion of stopped neutron energy, which approximately doubles the fusion gain. Finally, the recovery of the expanded liner makes a contribution ($\sim 5\% - 20\%$) to the overall energy output of the system.

In the gain calculations, we chose a compressed target density of 10^{28} m^{-3} to estimate what would be needed for $G_{\text{system}} \sim 1$ without secondary burn of liner material. Accounting for secondary burn of the liner is beyond the scope of the present work but could substantially increase the gain. Sufficient liner heating is not limited to alpha deposition, and may occur via several other mechanisms, including thermal conduction and radiative transport from the target, alpha deposition in the magnetic diffusion layer at the liner/target boundary, and shock heating of the liner.

VI. CONCLUDING REMARKS

PLMIF is a fusion energy concept that utilizes an imploding plasma liner to shock heat and compress a magnetized target plasma to fusion conditions. The plasma liner approach seeks to address some of the engineering concerns of the solid liner approach since liner formation is repeatable on a time scale limited only by the chamber evacuation time and recharge time on the capacitor bank. A number of theoretical issues need to be addressed in further detail, such as the stability of the compression and the flux conserving properties of the liner.

Recent theoretical results[18] suggest that the dwell time for a target confined by a plasma liner is of the order of 100 ns, which would significantly limit the fusion yield produced by the burning target. We used the exact solution to the self-similar converging shock model to show that the dwell time for the same conditions may actually be an order of magnitude longer from 750 to 4700 ns. There are several reasons for the longer time. First, the expansion velocity of the target is only about 2%–5% of the incoming liner velocity. Thus, the dwell time of the target is going to be determined by the sum of the outgoing shock and rarefaction times. The propagation time of the outgoing shock, which causes liner stagnation, was conservatively estimated to be $\ell/2v_l$, where ℓ is the liner thickness and v_l is the liner velocity, and this served as a lower limit on the calculated dwell time.

The engineering gain was found to be ∼1.7. Several important factors contribute to a gain exceeding unity. The longer dwell time leads to a higher fusion fuel burn-up fraction. Including the thermal recovery of the neutron energy roughly doubles the fusion gain, while the contribution from the liner recovery is between 5% and 20%. We make a final remark that this analysis neglects the bootstrap burn of the liner which may be enabled by several transport mechanisms and may contribute significantly to the fusion power.

ACKNOWLEDGMENTS

[1] M. M. Basko, A. J. Kemp, and J. Meyer-ter-Vehn, Nucl. Fusion **40**, 59 (2000).

[2] R. C. Kirkpatrick, I. R. Lindemuth, and M. S. Ward, Fusion Technol. **27**, 201 (1995).

[3] R. E. Siemon, I. R. Lindemuth, and K. F. Schoenberg, Comments Plasma Phys. Controlled Fusion **18**, 363 (1999).

[4] R. P. Drake, J. H. Hammer, C. W. Hartman, L. J. Perkins, and D. D. Ryutov, Fusion Technol. **30**, 310 (1996).

[5] T. P. Intrator, G. A. Wurden, P. E. Sieck, W. J. Waganaar, R. Renneke, L. Dorf, M. Kostora, S. C. Hsu, A. G. Lynn, M. Gilmore, R. E. Siemon, T. Awe, J. Degnan, C. Grabowski, and E. L. Ruden, J. Fusion Energy **27**, 57 (2008).

[6] O. V. Gotchev, N. W. Jang, J. P. Knauer, M. D. Barbero, R. Betti, C. K. Li, and R. D. Petrasso, J. Fusion Energy **27**, 25 (2008).

[7] A. Sherwood, *Megagauss Physics and Technology. Second International Conference on Megagauss Magnetic Field Generation and Related Topics*, Washington, D.C. (Plenum, New York, 1980), p. 375.

[8] Y. C. F. Thio, E. Panarella, R. C. Kirkpatrick, C. E. Knapp, and F. J. Wysocki, in *Proceedings of the Second Symposium, Current Trends in International Fusion Research*, Washington, D.C., 1997, edited by E. Panarella (NRC Research, Ottawa, 1999), p. 113.

[9] Y. C. F. Thio, C. E. Knapp, R. C. Kirkpatrick, R. E. Siemon, and P. J. Turchi, J. Fusion Energy **20**, 1 (2001).

[10] J. Cassibry, F. Thio, T. E. Markusic, and S. T. Wu, J. Propul. Power **22**, 628 (2006).

[11] D. Ryutov and Y. C. F. Thio, J. Fusion Energy **26**, 173 (2007).

[12] C. E. Knapp, "An implicit smooth particle hydrodynamic code," Ph.D. Thesis, University of New Mexico, 2000.

[13] Y. C. F. Thio, R. C. Kirkpatrick, C. E. Knapp, J. Cassibry, R. Eskridge, M. Lee, J. Smith, A. Martin, S. T. Wu, and G. Schmidt, in *Proceedings of the Fourth Symposium, Current Trends in International Fusion Research*, Washington, D.C., 2001, edited by C. Orth and E. Panarella (NRC Research, Ottawa, 2007), p. 465.

[14] H. B. Chen, L. Zhang, and E. Panarella, J. Fusion Energy **14**, 389 (1995).

[15] E. Panarella, J. Fusion Energy **6**, 285 (1987).

[16] Y. C. F. Thio and R. C. Kirkpatrick, Annual Meeting of the American Nuclear Society, Hollywood, Florida, 2002.

[17] S. C. Hsu, J. Fusion Energy **27**, 246 (2008).

[18] P. Parks, Phys. Plasmas **15**, 062506 (2008).

[19] Y. B. Zel'dovich and Y. P. Raizer, *Physics of Shock Waves and High-Temperature Hydrodynamic Phenomena* (Dover, New York, 2000).

[20] R. B. Lazarus and R. D. Richtmyer, Los Alamos Scientific Laboratory Report No. LA-6823-MS, 1977.

[21] R. D. Richtmyer and R. B. Lazarus, Los Alamos Scientific Laboratory Report No. LA-6108-MS, 1975.

[22] R. B. Lazarus, SIAM (Soc. Ind. Appl. Math.) J. Numer. Anal. **18**, 316 (1981).

[23] E. M. Lifshitz and L. D. Landau, *Fluid Mechanics*, Course of Theoretical Physics Vol. 6, 2nd ed. (Reed Educational and Professional Publishing, Boston, 1987), Chap. 10.

[24] R. H. Lovberg and C. L. Dailey, AIAA J. **20**, 971 (1982).

[25] P. G. Mikellides and C. Neilly, *40th AIAA/ASME/SAE/ASEE Joint Propulsion Conference and Exhibit*, Fort Lauderdale, Florida (AIAA, Reston, 2004).

[26] D. E. Johnson and D. P. Bauer, IEEE Trans. Magn. **25**, 271 (1989).